

Creep response of granular materials

Cécilia Gicquel, Ambroise Mathey, Jérôme Crassous, and Axelle Amon*

Univ Rennes, CNRS, IPR (Institut de Physique de Rennes) - UMR 6251, F-35000 Rennes, France

Abstract. We present an experimental study of creep deformation measured in a dry granular material submitted to a constant deviatoric stress smaller than its failure threshold. We observe creep deformation leading to material failure. An interferometric method of measurement of local strain allows us to observe how strain self-organizes in the sample from homogeneously distributed local plastic events to localization of the deformation in shear bands.

1 Introduction

Creep can be defined as a time-dependent process during which a material deforms, or even yields, when subjected to a constant stress below its strength limit. This phenomenon occurs in many materials, such as metals [1], rocks [2, 3], concrete [4, 5], paper [6], colloidal glasses [7] or granular materials [8–10]. Because of this universality, models that do not depend on the systems detail have been proposed to capture the behavior observed [11, 12]. Indeed, the strain response of materials in creep experiments generally follows the same phenomenology [3, 10]. In a first stage (primary creep, denoted I in Fig. 1), strain ϵ slows down with time. The strain rate $\dot{\epsilon}$ is observed to decrease as a power-law with time from the start of the stress-imposed condition: $\dot{\epsilon} \sim (t - t_0)^\alpha$ with $\alpha \simeq -1$ for most materials and in particular in granular materials [1, 3, 10].

In a second stage the strain rate reaches a minimum value (secondary creep, II in Fig. 1) and the strain evolves linearly with time. In a last stage (tertiary creep, III in Fig. 1), strain accelerates until failure of the material at time t_f . This stage of creep has been much less studied than creep I, as its observation requires experiments close to, but below, the failure threshold. This condition is necessary if creep failure is to be observed within a reasonable time from the point of view of experimental times. Working so close to the threshold is an experimental challenge for most materials. Experiments that have studied creep III have generally reported a power law for strain rate as a function of time remaining before failure: $\dot{\epsilon} \sim (t_f - t)^\beta$ with β also close to -1.

This phenomenology has been studied in granular materials, either in saturated or dry conditions, to determine the long-term stability of soils submitted to a constant load in civil engineering (e.g. [13]) and geophysical (e.g. [14]) contexts. The observation of primary creep is well established [8–10], but the subsequent regimes, in particular the possibility of spontaneous failure when the applied stress is below the material's failure threshold, have very rarely

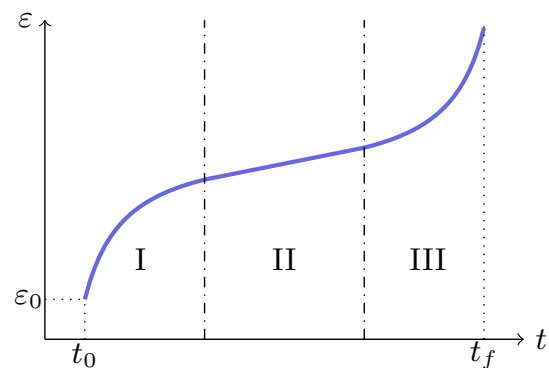


Figure 1. Strain ϵ as a function of time for a typical creep test at constant stress σ_0 . The stress-imposed condition starts at $t = t_0$ and is maintained constant until failure of the material at $t = t_f$. To reach σ_0 , a first stage of loading, generally at imposed strain, is needed until the setpoint is reached. The initial state of the sample is thus at a strain $\epsilon = \epsilon_0 \neq 0$. Typically, three regimes of creep strain are observed: deceleration (I), linear increase (II) and acceleration until failure (III).

been studied. When the confining pressure applied to the sample is low enough to prevent grain crushing, such instability has never been reported to our knowledge. In the latter case, the origin of the time-dependent internal processes is unclear. Indeed, creep deformation is a time-dependent process, which implies the existence of activation mechanisms within the material. Granular materials, defined as materials constituted of grains of diameter larger than $100 \mu\text{m}$, are considered as athermal. Dry and saturated granular materials are also characterized by the absence of cohesive bonds between the grains, so that no damage or fracture-like processes are expected.

The micromechanical processes at the origin of creep in granular materials are still unknown. Hypotheses put forward for activated mechanisms are either thermal or physico-chemical effects at the level of frictional contacts

*e-mail: axelle.amon@univ-rennes.fr

between grains [15], or the existence of residual vibrations acting as mechanical noise on the system [16, 17]. For granular materials subjected to low confining pressure, these processes should be linked to structural reorganization of the granular pile. Experiments to monitor internal changes are rare and based either on post-mortem studies of pile organization [18], or on indirect measurements based on acoustic emission [19].

A thorough study of the three phases of creep phenomenology in granular media is thus still needed. In this article we present creep experiments performed on a dry granular material. We observe the three phases of creep for imposed stresses below the failure threshold. Moreover, thanks to an interferometric method of micro-deformation measurement, we are able to monitor the spatial distribution of the strain in the sample at the different stages of creep.

2 Experimental setup

2.1 Principle of the biaxial test

At Institut de Physique de Rennes (IPR), we have developed a mechanical setup allowing us to perform biaxial tests on dry granular materials. The setup has been extensively described in several papers [20, 27]. The geometry of the test is represented Fig. 2 (left).

The sample studied is composed of glass beads placed in a latex envelope. A pressure difference, ΔP is applied by a vacuum pump between the inside of the envelope and the outside atmosphere. One side of the sample consists in a glass panel, allowing imaging of the sample. The prepared sample is then placed in the testing machine (Instron 5965 Dual Column Table Frame).

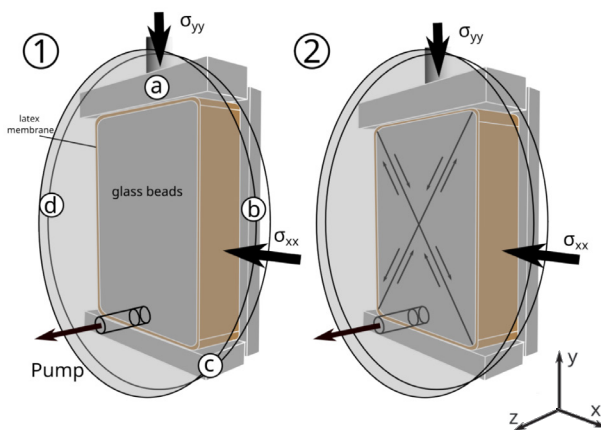


Figure 2. (Left) principle of the biaxial test. (a) translation stage; (b) metallic back plate; (c) bottom rigid plate; (d) glass panel. (Right) post-failure geometry with two conjugated shear bands with displacements represented relative to the sample center.

During the biaxial test, we aim to apply controlled stress $-\sigma_{xx}$ and $-\sigma_{yy}$ to two axes of our sample (defined in Fig.2), while the sample volume is free to change. The experiment is carried out in a plane strain geometry, with

strain along the z -axis considered zero because the sample is confined between the glass panel (2.1(d)) and a rigid back panel (2.1(b)) both fixed to the frame of the testing machine. The stress along the z -axis is not monitored. The stress along the x -axis is fixed by the confining pressure applied by the pump $-\sigma_{xx} = \Delta P$. A mechanical stress is applied by lowering a translation stage along the y direction (2.1(a)). It compresses the sample with a force F measured by a load cell (2580 Series 5 kN Static Load Cell from Instron). The stress along the y -axis is then $-\sigma_{yy} = \Delta P + F/A$, with A the top surface area of the sample. The macroscopic strain of the sample along the y -axis is given by the displacement u we either impose or measure: $\epsilon = u/L_y^0$ with L_y^0 the initial height of our sample and the vertical strain rate is denoted as $\dot{\epsilon}$. In strain rate imposed experiments $\dot{\epsilon} = v/L_y^0$ with v the velocity of the translating platform compressing the sample. We don't measure the volumetric strain in our experiments.

2.2 Spatial deformation measurements

To observe the deformation occurring in the sample, we use an optical interferometry technique called Diffusive Wave Spectroscopy (DWS). The method has been described in detail in [21, 22]. It gives access to spatially resolved maps displaying the local incremental strain occurring in the sample between two states ϵ and $\epsilon + \delta\epsilon$, examples of which are shown in Fig. 3. The strain maps are the result of computation of correlations $g_I(x, y, \epsilon, \epsilon + \delta\epsilon)$ between speckle images of the sample taken at different times, and thus in different strain states. It is different from Digital Image Correlation (DIC). In our case, the correlation is computed at the same position (x, y) and it is the local loss of correlation during the time interval which is evaluated, with $g_I = 1$ (respectively $g_I = 0$) for correlated (resp. decorrelated) speckle patterns. By modeling the light propagation in the scattering sample, a scalar strain γ , which is a function of the quadratic invariant of the local strain tensor, can be deduced from g_I [21, 22]: $\gamma = -\frac{\ln g_I}{C}$ with $C \approx 3.6 \times 10^3$ for our optical system [27]

2.3 Typical strain-imposed experiment

We first detail the typical response of a sample for a strain-imposed experiment. Fig. 3 (bottom) shows the stress deviator $\sigma_{xx} - \sigma_{yy}$ as a function of the sample vertical strain ϵ . This stress-strain curve displays an increase of the stress until a peak value σ_P before reaching a plateau.

The strain maps shown in Fig. 3 (top) display the local strain γ in the sample at different values of ϵ , with areas of low strain in white and areas of high strain in black. We observe that the local strain is spread out over the whole sample during the initial increase of the deviatoric stress. Once the strain of the sample ϵ reaches a value between 3 to 4 %, corresponding to the position of the peak σ_P , the deformation inside the sample localises in shear bands separating the sample in solid blocks sliding against each other ("X" pattern for $\epsilon > 4\%$ in Fig. 3, blocks kinematics schematically represented Fig. 2.2). Interestingly, at all the stages of the test, the local strain γ occurs mostly in

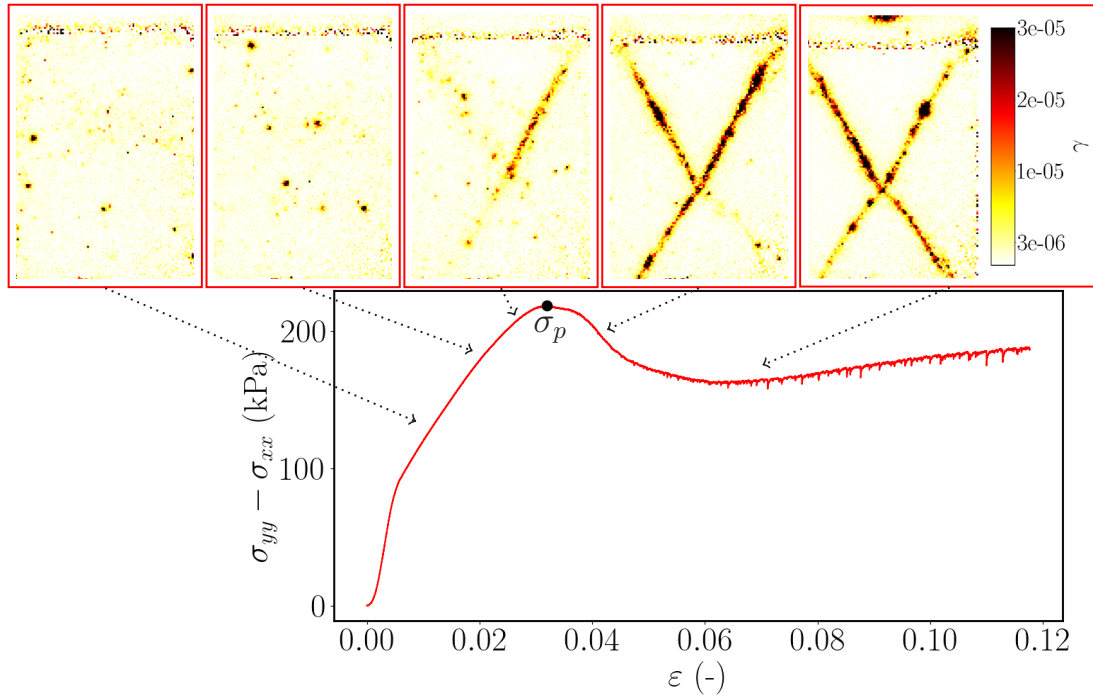


Figure 3. Deviatoric stress $\sigma_{xx} - \sigma_{yy}$ as a function of the sample strain ϵ for a typical strain imposed experiment with $-\sigma_{xx} = \Delta P = 30$ kPa. Inserts: Strain maps at different values of ϵ ($\delta\epsilon = 5.8 \times 10^{-7}$).

the form of dark spots (maps top of Fig. 3), meaning that the deformation follows a discrete dynamics. We call these clusters of strain *plastic events* as the strain of the sample is always plastic. For $\epsilon < 3\%$, the events are spread over the whole sample. For $\epsilon > 4\%$, the shear bands appear as multiple events occurring along fixed direction.

We have extensively studied the spatial organization of the plastic deformation during strain-imposed experiments [23–25] as well as the statistical properties of the plastic events [26–28] in previous works done at IPR. In particular, we have quantitatively compared the spatio-temporal properties of the plastic events to earthquakes dynamics [26, 28], unveiling the rate independence of aftershock sequences in both systems [28]. Local, intermittent, rearrangements have also been observed recently in numerical simulations [29–31] in which self-organization of the deformation at different scales have been observed similar to the one we observe in our experiments.

In the present article we present results obtained using this setup in stress imposed conditions $\sigma_0 < \sigma_p$ and study the creep strain that takes place in the material.

3 Force imposed experiments

3.1 Setup

The commercial device we use for mechanical testing (Instron 5965) enables us to carry out imposed-force test protocols. The test is controlled via the commercial software (“bluehill”) of Instron. The underlying principle is the use of a PID feedback loop. In practice, the only adjustable parameter of the loop we can tune in the software is the

proportional parameter P that we have adjusted to minimize the oscillations of the force around the force setpoint. Typically those oscillations have an amplitude of 0.05% of the setpoint value. Note that our experiments are force-imposed experiments and not stress-imposed ones. As the cross-section of the sample increases during test, the imposed stress decreases.

3.2 Choice of the setpoint

An important issue in stress or force imposed experiments is the choice of the setpoint value (deviatoric stress σ_0). This must be defined in relation to the peak of the loading curve σ_p of the granular material. It is therefore necessary to prepare the samples in such a way as to ensure reproducibility of the loading curve, and therefore with a similar internal organization of the granular medium from one test to the next. A second point is to be able to perform creep experiments over timelapse reasonable at the scale of laboratory experiments (typically a maximum of a few days). It is well known [8–10] that strain rate in stress imposed experiments increases with the value of the stress setpoint. Thus, when the imposed stress is much smaller than the yield stress, the time to failure in the corresponding stress-imposed experiment can be unreasonably long. Literature reports that good choices for the setpoint are values between the onset of dilatancy and value of the peak σ_p [3, 32]. In our setup we don’t have access to the volumetric strain. We chose setpoint values between the plateau value of the stress in the critical state and the peak stress as such values correspond to bistable states of the material.

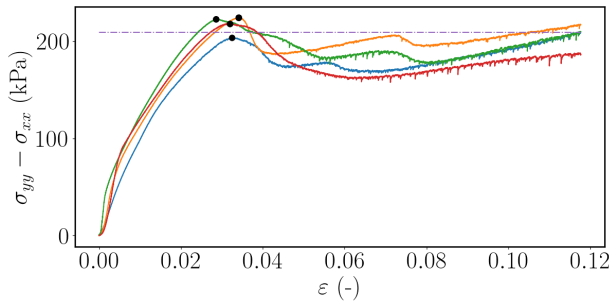


Figure 4. Loading curves for strain-rate imposed experiments performed on dense granular samples prepared with the protocol described in section 3.3. Confining pressure $\Delta P = 30$ kPa, $\langle \sigma_p \rangle = 217$ kPa, $\text{std}(\sigma_p) = 8$ kPa.

3.3 Preparation of the granular material

To obtain a reproducible loading curve with a well-defined peak stress, we prepare granular samples close to random close packing. A sample preparation protocol was therefore developed, based on the use of mechanical vibrations imposed by taps using a mass connected to a shaker.

Preparation takes place in several stages. A mass of 160 ± 1 g of glass beads is poured into the membrane which is placed in a holder, then this holder is submitted to taps (frequency 10 Hz) during 40 minutes. An additional 20 ± 1 g of beads is then added to fill the membrane to the brim, and taps resume for 10 minutes. Finally, an adjustment is made manually to ensure that the corners of the membrane are sufficiently filled and that the sample surface is flat. The glass panel (Fig. 2.1.d) can then be placed at the top of the sample to proceed at its depressurization ($\Delta P = 30$ kPa).

Figure 4 shows the loading curves obtained in strain-rate imposed conditions for samples prepared following the above preparation protocol. A very good repeatability is obtained allowing to define a mean for the peak value $\langle \sigma_p \rangle$ with a standard deviation $\text{std}(\sigma_p)$ such than $\text{std}(\sigma_p)/\langle \sigma_p \rangle \simeq 4\%$.

4 Creep response at constant load

4.1 Measurements

We performed stress-imposed experiments at a value $\sigma_0 = \sigma_p - \text{std}(\sigma_p) = 0.96\sigma_p$. A typical strain response ϵ as a function of time t is shown Fig. 5 (left). The strain increases between time t_0 , which marks the beginning of the stress-imposed protocol and $t_4 = t_f$ which corresponds to the failure of the sample. To the best of our knowledge, those experiments are the first observation on drained granular samples, without crushing of grains, of failure of the sample while imposing stress smaller than the peak stress. Indeed, previous experiments at low confining pressures displaying acceleration of the strain to failure were performed with $\sigma_0 > \sigma_p$ [8, 10].

A surprising feature is visible in Fig. 5. The strain response presents discontinuities at times t_1 , t_2 and t_3 so that

the measured signal is formed of successive steps (denominated by a colored number in Fig. 5). This feature has been observed in all the experiments we have performed but the number of steps is variable from one experiment to the other. In the following, times t_i are defined as the inflection points of the curve, obtained by derivation and filtering of the signal. Note that different window definition options are possible in order to study each step individually, e.g. the middle of the plateaus could have been used instead of the inflection points. In our approach, each step considered individually, as in Fig. 5 (right), presents the features of a three-phase creep process: first an increase of the strain at a decelerating strain rate (primary creep, I in Fig. 5 (right)), then a linear increase of the creep (creep II) and finally an acceleration of the strain (creep III). Surprisingly, these accelerations do not lead to failure for the three first steps. Consequently, the internal rearrangements that occur in the sample during deformation jumps are probably of a different nature to those that trigger material failure. In what follows, we will nevertheless compare the strain rates during intermediate acceleration phases with the final acceleration to determine whether the dynamics during acceleration phases are similar.

Thanks to our spatially-resolved method of measurement of local strain, we can check the spatial distribution of the strain during the creep process. Inserts of Fig. 5 show maps obtained at different times (indicated by arrows on the $\epsilon(t)$ curve). Those maps correspond to the strain occurring between times t and $t + \delta t$ with δt fixed by the framerate of the camera ($\delta t = 200$ ms). As $\dot{\epsilon}$ is not imposed, the strain occurring during that time interval is not constant from one map to another, in opposition to the maps shown in strain rate imposed experiments (Fig. 3) for which a fixed δt corresponds to a fixed $\delta \epsilon = \dot{\epsilon} \delta t$.

In Fig. 5, we observe that at the level of the first steps t_1 and t_2 , the local strain γ in the sample takes the form of localized events (the dark “spots”) homogeneously distributed in the sample. This spatial distribution is the same as the one observed before failure when performing strain-imposed experiments (see Fig. 3 for $\epsilon_M < 3\%$). At $t = t_3$ (Fig. 5) most of the events are concentrated along two conjugated lines. Still, at this stage, the acceleration of the strain does not lead to failure and between t_3 and t_4 the structuration of the strain field vanish. Then, at $t = t_4$, deformation is again localized along two conjugated lines forming shear bands and failure takes place.

4.2 Analysis of the strain-rate dynamics

We have studied the strain-rate $\dot{\epsilon}$ dynamics in the decelerating and accelerating phases at the level of all the steps. The strain-rate is computed by numerical differentiation of $\epsilon(t)$ followed by averages on logarithmic steps. We plot in Fig. 6(a) $\dot{\epsilon}$ as a function of $(t - t_i)$ to study the decelerating parts of the strain and in Fig. 6(b) $\dot{\epsilon}$ as a function of $(t_{i+1} - t)$ to study the accelerating parts. The colors of the curves correspond to the colors associated to the number of the step in figure 5.

We observe that for all the steps the strain rate follows a power law in the two regimes (creep I and III). The ex-

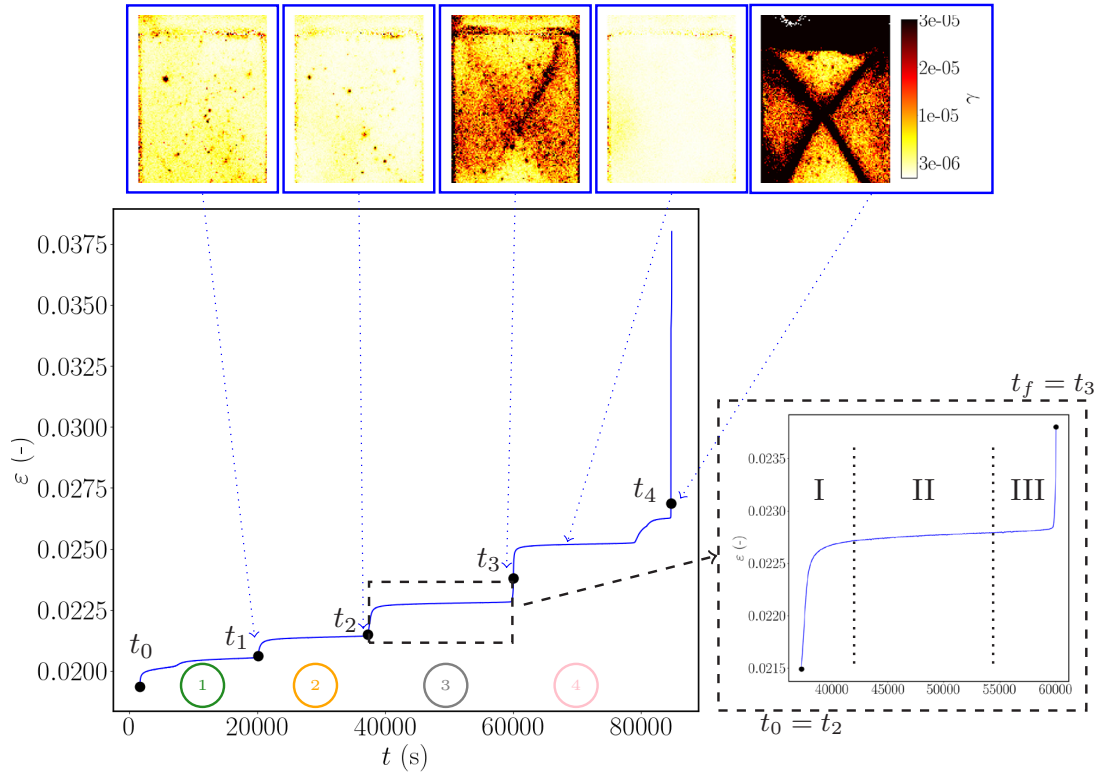


Figure 5. Main graph: macroscopic strain ϵ measured during a stress imposed experiment with deviatoric stress $\sigma_0 = 209$ kPa and $\Delta P = 30$ kPa. Inserts: strain maps displaying local strain γ obtained at different times and for time increments $\delta t = 200$ ms. Right: close-up of step n°3.

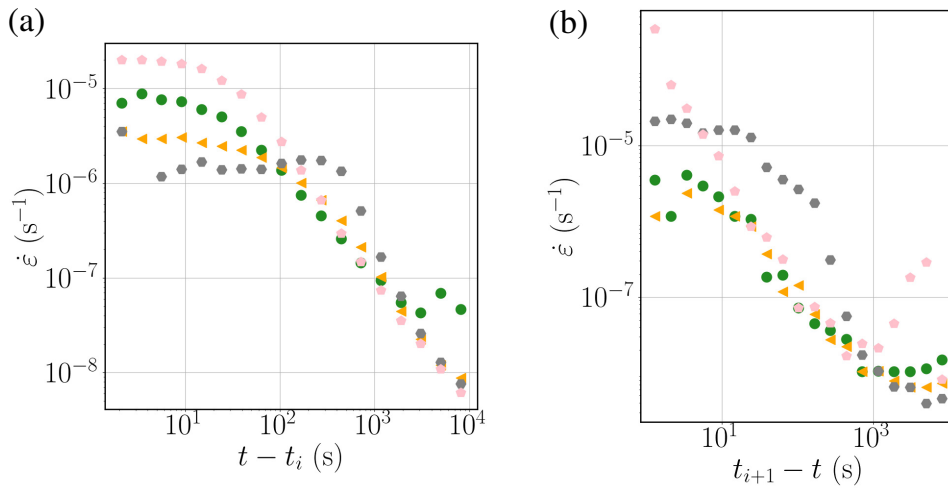


Figure 6. Strain rate $\dot{\epsilon}$ as a function of a. $(t - t_i)$ (creep I), b. $(t_{i+1} - t)$ (creep III). t_i s are defined in Fig. 5 and correspond either to the beginning or the end of the creep process for a given step. Each curve corresponds to one of the step with the colorcode given by the numbering of the steps in Fig. 5.

ponent in the case of creep I is close to -1 in agreement with the exponent observed in previous experiments [8–10] and this behavior of the strain is observed after each discontinuities when slowing down of the strain resumes after a temporary acceleration. In the case of creep III, the exponent β of the power-law $(t_{i+1} - t)^\beta$ is steeper than -1. Note that the values of $\dot{\epsilon}$ are close to our resolution limit.

4.3 Discussion

In our stress controlled experiments, we observe globally the same phenomenology as observed in other materials: creep strain with a non-monotonous strain-rate with first a deceleration of the strain with $\epsilon \sim (t - t_0)^{-1}$, second a linear increase and third a final acceleration towards failure with $\epsilon \sim (t_f - t)^\beta$. The exponents characterizing the accel-

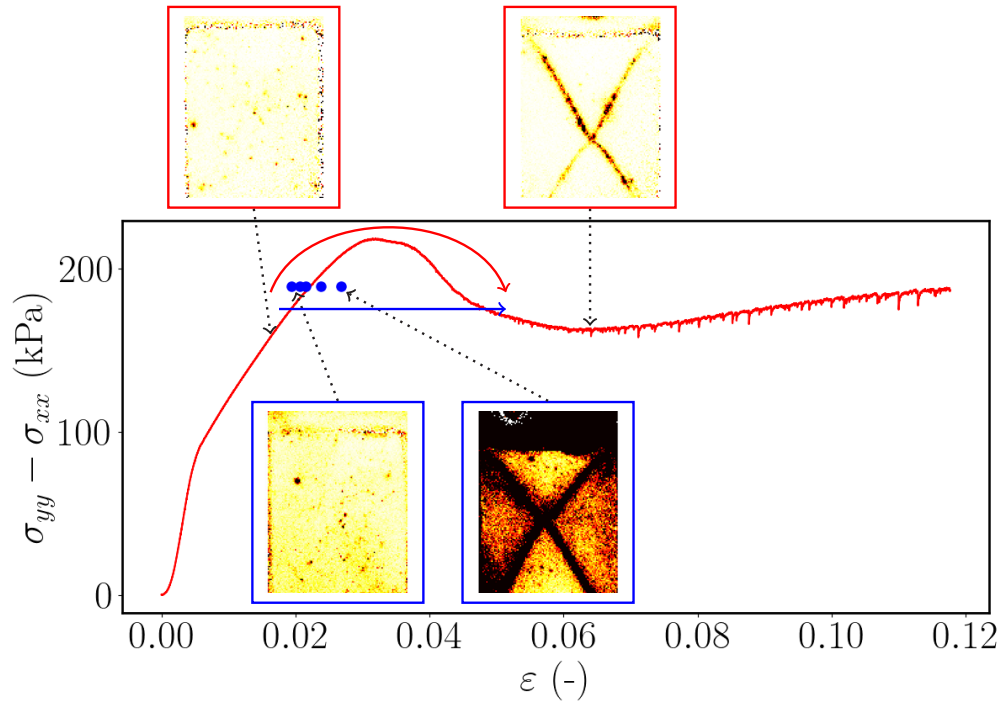


Figure 7. Stress-strain curve obtained at imposed strain rate (red curve) and strains at time t_i in imposed stress experiment (blue dots). Inserts: strain maps observed for strain-rate imposed experiments (red frame) and stress imposed experiments (blue frame).

erating and decelerating phases are of the same order as observed in other types of materials.

The spatial distribution of the local strains during creep is comparable to the one observed in strain-imposed experiments. Consequently, the process of self-organisation of the deformation from homogeneously plasticity distributed spots to localization of the deformation in shear bands does not depend of the loading mode. This observation is synthesized in Fig. 7 where the stress-strain curve obtained at imposed strain rate (in red) and the value of the strain at times t_i of the imposed stress experiment (in blue) are superimposed. This observation is reminiscent of observations of the spatial structuration of deformation field in numerical simulations [32] where the creep process is reproduced by implementing creep at the level of the frictional contacts between the spheres [15].

A specificity of our observation is the presence of discontinuities (“steps”) in our strain response. Similar features have been observed in another heterogeneous material displaying creep at imposed stress: crumpled sheets [33]. The authors of this study interpret the discontinuities of the displacement as cascades of correlated events in the system which generate large displacement events.

5 Conclusion

To conclude we have observed the three phases of creep deformation in a dry granular material at low confining pressure submitted to a constant deviatoric stress smaller than its peak stress, up to spontaneous failure in the material. Our spatially resolved strain measurement method

enables us to observe the organization of deformation in the sample. We observe localized plastic events homogeneously distributed in the sample at the beginning of the creep process and shear bands formation at the end. A surprising feature we observe in the macroscopic strain curve is the presence of discontinuities. Spatially resolved deformation measurements show that with each successive discontinuity, deformation becomes increasingly localized.

We are currently studying deformation maps to quantify the spatial distribution of strain and compare this distribution with that observed and characterized in imposed strain experiments [20, 23–25]. The next step will be to identify the driving force behind the activation process. An interesting perspective is the role of mechanical noise in the system [16, 17]. Can vibrations play the role of an effective temperature? To answer this question, we intend to inject mechanical noise into the system and compare its effect on creep with that of a temperature increase on a thermal system.

Acknowledgements

This work has been supported by the French National Research Agency through the project DISCREEP (Grant ANR-23-CE30-0031).

References

- [1] E. N. da C. Andrade, *On the viscous flow in metals, and allied phenomena*, Proc. R. Soc. A, **84**, 1 (1910)
- [2] C. H. Scholz, *Mechanism of Creep in Brittle Rock*, J. Geophys. Res., **73**, 3295 (1968)

- [3] N. Brantut, et al. *Time-dependent cracking and brittle creep in crustal rocks: A review*, J. Struct. Geol., **52**, 17 (2013)
- [4] F. P. Zhou, *Time-dependent crack growth and fracture in concrete*, Lund University, Lund, Sweden (1992)
- [5] Z. P. Bazant, in *Materials Science of Concrete IV* edited by J. Skalny and S. Mindess (The American Ceramic Society, 1995) pp. 355-389.
- [6] J. Koivisto et al., *Predicting sample lifetimes in creep fracture of heterogeneous materials*, Phys. Rev. E, **94**, 023002 (2016)
- [7] M. Siebenburger et al., *Creep in Colloidal Glasses*, Phys. Rev. Lett, **108**, 255701 (2012)
- [8] S. Murayama, K. Michihiro, and T. Sakagami, *Creep characteristics of sands*, Soils Found., **24**, 1-15 (1984)
- [9] P. V. Lade and C.-T. Liu, *Experimental study of drained creep behavior of sand*, J. Eng. Mech., **124**, 912-920 (1998)
- [10] A. Augustesen, M. Lingaard, and P. V. Lade, *Evaluation of Time-Dependent Behavior of Soils*, Int. J. Geomech., **4**, 137 (2004)
- [11] D. F. Castellanos, and M. Zaiser, *Avalanche behavior in creep failure of disordered materials*. Phys. Rev. Lett., **121**, 125501 (2018)
- [12] J. Weiss, and D. Amitrano, *Logarithmic versus Andrade's transient creep: Role of elastic stress redistribution*. Phys. Rev. Mat., **7**, 033601 (2023)
- [13] J. K. Mitchell and K. Soga, *Fundamentals of Soil Behavior* (John Wiley & Sons, New York, 2005) 3rd edition
- [14] N. S. Deshpande, et al., *The perpetual fragility of creeping hillslopes*, Nat. Commun. **12**, 3909 (2021)
- [15] M. R. Kuhn and J. K. Mitchell, *New perspectives on soil creep*, J. Geotech. Engrg., **119**, 507-524 (1993)
- [16] D. Espindola, B. Galaz and F. Melo, *Ultrasound Induces Aging in Granular Materials*, Phys. Rev. Lett., **109**, 158301 (2012)
- [17] A. Pons et al., *Mechanical fluctuations suppress the threshold of soft-glassy solids: the secular drift scenario*, Phys. Rev. E, **92**, 020201 (2015)
- [18] E. T. Bowman and K. Soga, *Creep, ageing and microstructural change in dense granular materials*, Soils Found., **43**, 107-117 (2003)
- [19] B. Bock, S. Vogt and R. Cudmani, *Acoustic emissions during creep under triaxial compression*, E3S Web Conf., **544**, 01006 (2024)
- [20] A. Le Bouil et al., *A biaxial apparatus for the study of heterogeneous and intermittent strains in granular materials*, Granular Matter, **16**, 1-8 (2014)
- [21] M. Erpelding, A. Amon, and J. Crassous, *Diffusive wave spectroscopy applied to the spatially resolved deformation of a solid*, Phys. Rev. E, **78**, 046104 (2008)
- [22] A. Amon, A. Mikhailovskaya, J. Crassous, *Spatially resolved measurements of micro-deformations in granular materials using diffusing wave spectroscopy*, Rev. Sci. Instrum. **88**, 051804 (2017)
- [23] A. Le Bouil et al., *Emergence of cooperativity in plasticity of soft glassy materials*, Phys. Rev. Lett., **112**, 246001 (2014)
- [24] T. B. Nguyen and A. Amon, *Experimental study of shear band formation: Bifurcation and localization*, EPL **116**, 28007 (2016)
- [25] D. Houdoux, et al., *Plastic flow and localization in an amorphous material: experimental interpretation of the fluidity*, Phys. Rev. E, **98**, 022905 (2018)
- [26] D. Houdoux, et al., *Micro-slips in an experimental granular shear band replicate the spatiotemporal characteristics of natural earthquakes*, Commun. Earth Environ., **90**, 2 (2021)
- [27] A. Mathey, et al. *A device for studying elementary plasticity fluctuations in granular media*, arXiv preprint arXiv:2403.09396 (2024)
- [28] A. Mathey et al., *Aftershocks as a time independent phenomenon*, Geophys. Res. Lett. **52**, e2024GL112618 (2025)
- [29] A. Clerc et al., *Meso-scale signatures of inertial transitions in granular materials*, Granular Matter, **23**, 28 (2021)
- [30] J. Liu et al., *Incremental shear strain chain: a mesoscale concept for slip lines in 2D granular materials*, Granular Matter, **24**, 119 (2022)
- [31] S. Luding, *Elastic-plastic intermittent rearrangements of frictionless, soft granular matter under very slow isotropic deformations*, Front. Phys. **11**, 1211394 (2023)
- [32] J. Wang and Z. Xia, *DEM study of creep and stress relaxation behaviors of dense sand*, Comput. Geotech., **134**, 104142 (2021)
- [33] Y. Lahini, S. M. Rubinstein, and A. Amir, *Crackling Noise during Slow Relaxations in Crumpled Sheets*, Phys. Rev. Lett., **130**, 258201 (2023)